Heating and Cooling of Ligand-Coated Colloidal Nanocrystals in Solid Films and Solvent Matrices

Journal:	*Nanoscale*
Manuscript ID	NR-ART-02-2019-001473.R1
Article Type:	Paper
Date Submitted by the Author:	28-Mar-2019
Complete List of Authors:	Diroll, Benjamin; Argonne National Laboratory, Center for Nanoscale Materials Schaller, Richard; Argonne National Laboratory, Center for Nanoscale Materials

SCHOLARONE™
Manuscripts

Heating and Cooling of Ligand-Coated Colloidal Nanocrystals in Solid Films and Solvent Matrices

Benjamin T. Diroll[*a] and Richard D. Schaller[a,b]

Ligand-to-nanocrystal heating and subsequent cooling to the environmental medium is investigated with infrared pump, electronic probe (IPEP) spectroscopy. Compared to solid films, solvated nanocrystals show faster ligand-to-nanocrystal heat equilibration (c. 11 ps versus c. 17 ps). Solvated nanocrystals also display more cooling of the hot ligand-nanocrystal complex on the experimentally measured time-scale, emphasizing the thermally insulating nature of semiconductor nanocrystal solids. Although heating transfer rates among solvents are all between 150 ps and 330 ps, cooling of the nanocrystal-ligand complex is slower, on average, in chlorinated solvents (c. 315 ps) compared to deuterated hydrocarbon solvents (c. 215 ps). Differences between chlorinated and hydrocarbon solvents show the importance of matching the vibrational energies of the solvent and the ligands for increasing the rate of heat transfer. Increases in the cooling time for poorer hydrocarbon solvents, in which nanocrystals aggregated, such as toluene, compared to better solvents, like methylcyclohexane, indicate that penetration of solvent into the ligand layer facilitates improved heat transfer to the matrix.

Introduction

The transfer of heat to and from devices places practical limits on their performance. As nanocrystal-based optoelectronic devices mature, management of heat plays an increasing role in the viability of technologies like downconversion phosphors,[1–3] light-emitting diodes,[1,4] and nanocrystal-based lasers,[5] and centrally impacts use in photothermal therapies[6] and thermoelectrics.[7] In many such systems, significant thermal loads may be anticipated, but little understanding exists regarding how the environment or matrix will affect the thermal properties of semiconductor nanocrystal compositions. Some limited studies have demonstrated extremely low "bulk" thermal conductivities in ligand-coated[8] and annealed nanocrystal solids.[9] A larger body of time-resolved spectroscopic studies performed on metallic, plasmonic nanocrystals have found heat outcoupling to solvent occurring on a time-scale of hundreds of picoseconds.[10–16] In earlier pump-probe measurements, electronic excitations generate heat in the nanoparticle typically by exciting at a localized surface plasmon resonance; this type of measurement cannot be used for non-degenerate semiconductors. Structural measurements, such as transient X-ray diffraction,[17] provide estimates of heat outflow for some semiconductor systems (on a similar time-scale), although generally these must be performed at high excitation densities.

This work uses infrared pump, electronic probe (IPEP) spectroscopy of semiconductor nanoplatelets (NPLs) dissolved in different solvents and as a solid film to examine the environmental effects on heat flow both from ligands to nanocrystals and from the ligand-nanocrystal complex to the surrounding medium. Compared with other pump-probe methods which have been used to study thermal transport, IPEP measurements do not require an electronic excitation, and therefore the spectroscopic signature reflects dynamics of phonons or vibrations without additional signals arising from electronic state filling.

Results and Discussion

Details of the sample used in this study appear in Figure 1. The same batch of 4 monolayer (ML) CdSe NPLs capped with oleic acid was used for all studies to control for size and ligand graft density effects—which may be substantial[14,18,19]. The absorption of the 4 ML CdSe NPLs in carbon tetrachloride reflects the heavy and light hole bands at 0.512 µm and 0.479 µm, respectively.[20] The hydrocarbon stretches of the oleate ligands absorb near 3.5 µm, but the CdSe itself is transparent in this region. Thermogravimetric analysis measurements (Figure S1) indicate that the NPLs used in this work have a ligand graft density of 1.8 ligands/nm^2. From our earlier report,[21] NPLs represent excellent samples for this type of measurement due to their large surface-to-volume ratios, which yield more ligand coverage per nanocrystal volume, and exceptionally narrow absorption resonances, which enhance sensitivity to subtle changes in energy. For example, the sample shown in Figure 1b has average lateral dimensions of 17.7±1.3 nm by 11.8±1.2 nm and a thickness of 1.4 nm.

In IPEP measurements, a IR pump pulse (Figure S2) is used to excite vibrations of the oleate ligands, inducing heating of the ligand modes through intramolecular vibrational relaxation.[22] Subsequently, heat is transferred from the hot ligand to the comparatively cold nanocrystal, resulting in a change in the band gap

a. Center for Nanoscale Materials, Argonne National Laboratory, Lemont, IL 60615.
b. Department of Chemistry, Northwestern University, Evanston, IL 60208
*bdiroll@anl.gov

ARTICLE   Journal Name
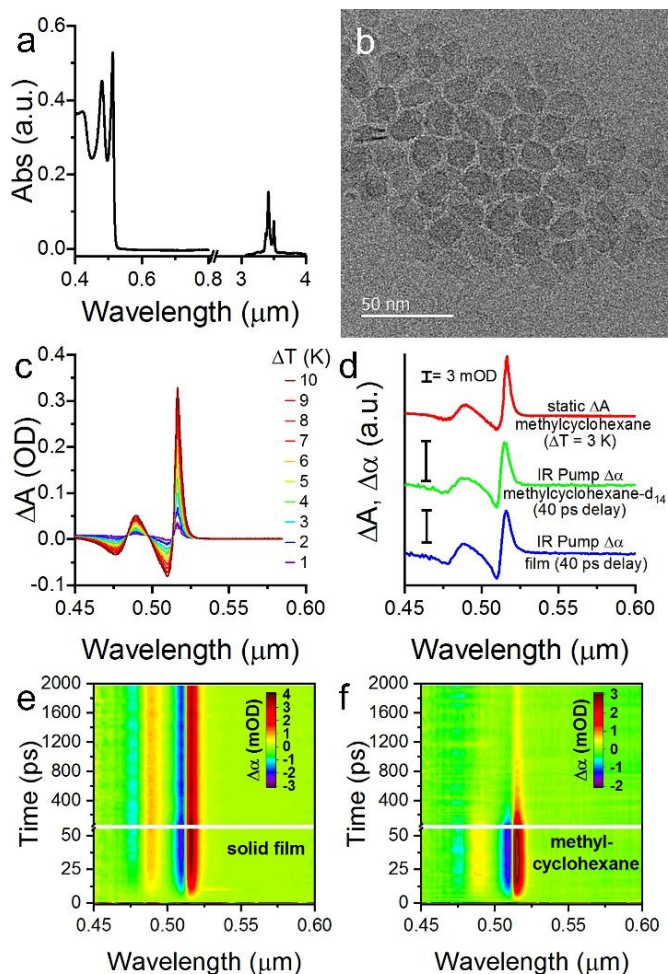

Figure 1. (a) Visible and infrared absorption of 4 ML CdSe NPLs used in this work, dissolved in carbon tetrachloride. (b) Representative TEM images of the NPL sample used in this work. (c) Static change in absorption spectra for increased temperatures, referenced to the spectrum at 295 K. (d) Static change in absorption spectra (ΔA) and transient IPEP spectra (Δα) of the same 4 ML CdSe NPL sample. (e, f) Two-dimensional maps of the temporal and spectral response of 4 ML CdSe NPLs to 3.46 μm pump excitation as a solid film (e) and in methylcyclohexane- d_{14}.

evidenced here via a bathochromic shift of the absorption resonances. Static absorbance changes (ΔA) for different static temperature changes (ΔT), referenced to absorption at 295 K in Figure 1c, confirm the red-shift with heating. Figure 1d shows static absorbance changes alongside transient absorption (Δα) spectra in IPEP experiments obtained at 40 ps delay for particles in a solvent or as a film. The nearly identical spectral shape of the static experiment and the IPEP experiment confirms that the infrared pump induces a thermal excitation in the inorganic nanocrystal.

Two-dimensional transient spectral maps of the IPEP experiment performed on a drop-cast film of the 4 ML CdSe NPLs and the same sample in methylcyclohexane-d_{14} are shown in Figures 1e and 1f, respectively. As with all hydrocarbon and hydrogen-containing solvents used in this work, a deuterated form was used to avoid, as much as possible, overlap with the absorption resonances of oleic acid C-H stretches. The rise of the IPEP Δα signal tracks the ligand-to-nanocrystal heat transfer process and the decay of the signal tracks the loss of heat from the ligand-nanocrystal complex to the surroundings. The signals of solid films and solution diverge
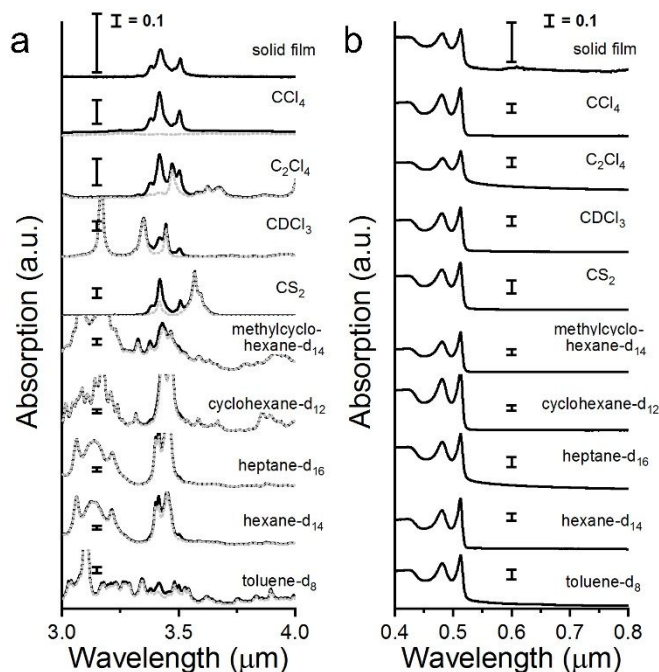

Figure 2. (a) FT-IR data of the 4 ML CdSe NPLs in different solvents, covering the spectral region of the ligand C-H vibrational absorption resonances and the infrared pump beam. The absorption spectra of the NPL samples are shown in solid black and the absorption of the solvent is shown in gray dashed lines. (b) Visible absorption of 4 ML NPLs in the same solvents. Measurements were performed in 1 mm quartz cuvettes.

substantially at delay times longer than 50 ps This large difference in the cooling of the nanocrystals was noted previously,[21] but the extent to which different solvents influence and impact the dynamics of heat transfer remain largely unexplored.

There are several models of interfacial heat transfer, but in all cases it is understood to depend on the energies and densities of phonon states on both the hot and cold side of an interface.[23–25] Interfaces in which materials have similar phonon density of states are expected to have high interfacial thermal conductance and those with poorly matched phonon density of states, such as inorganic nanoparticles and organic ligand coatings[8,26] or self-assembled monolayers,[27] have low interfacial thermal conductance. Introducing a solvent, which may penetrate the ligand layer, adds additional complexity to interfacial heat conduction.[19,28] Solvent molecules may displace ligands and alter their orientation, both which can affect the rate of interfacial transfer. Less ambiguously, solvents transfer heat from the nanoparticle-ligand complex by diffusing away from the surface while in a vibrationally hot state (See Supporting Information Figure S3). This is, for example, clear from the comparison of the dynamics at longer delay times in Figures 1e and 1f: the ligand-only matrix of a solid nanocrystal film is insufficient to transport heat away from the nanocrystal on a sub-nanosecond time-scale.[8] Engineering alignment of ligand layers or use of additives to facilitate thermal transport may facilitate improved cooling to the benefit of devices. Use of different solvents can offer insights into the molecular engineering desired for enhanced cooling of nanocrystal-ligand complexes. For example, one particularly significant finding from molecular dynamics simulations of solvent-nanocrystal interfaces, perhaps intuitive from enhances in thermal transport of
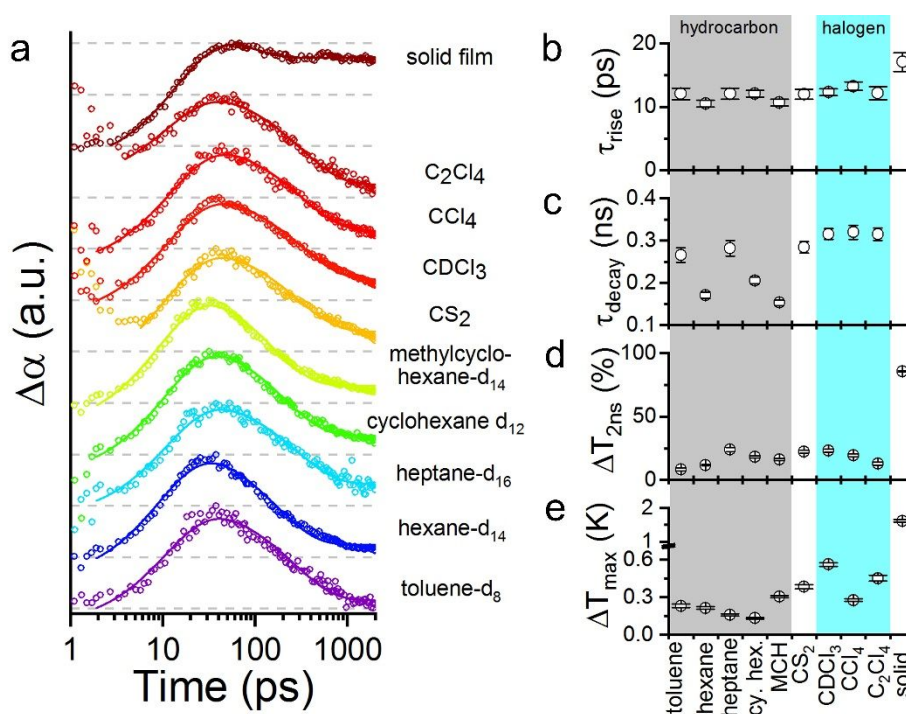
Figure 3. (a) Open circles show line-cuts at the heavy-hole induced absorption of the 4 ML CdSe NPLs in IPEP experiments in different matrices. Solid lines show a convoluted fit of the heating rise time and cooling decay time. Dashed lines indicate a value of Δα = 0 for offset scans. (b) Rise times fitted from IPEP heavy hole bleach features. (e) Decay times fitted from IPEP heavy hole bleach features. (d) Percentage of heat loss at 2 ns delay time compared to the maximum observed ΔT in the IPEP experiment for each sample. Error bars of (b)-(d) are provided based upon fitting error. (e) Maximal temperature rise estimates based upon IPEP spectra. Error bars are provided based upon noise of the IPEP spectral data at the maximal temperature change point.

aligned polymers,[29] is that better matching of the molecular director of the ligands and solvent facilitate heat transfer from the nanoparticle-ligand complex to the surrounding matrix. This work exploits the dispersibility of oleic acid coated nanocrystals in many solvents to explore the variability in heating and cooling within different environments. Solution FT-IR absorption spectra are shown in Figure 2a and the corresponding visible absorption spectra for the dissolved NPLs are shown in Figure 2b. Although the solvents are deuterated, those with lower deuteration purities have strong infrared absorptions at the same energies as the oleic acid C-H stretches, evidenced by the gray dashed lines in Figure 2a. Nonetheless, the samples still display at least some additional absorption in all cases, particularly on the wings of the C-H stretching features.

Another unexpected consideration arising in these experiments was the difference in solubility between natural abundance and deuterated solvents. Optical absorption spectra in Figure 2b and TEM images confirm (Supporting Information Figure S4) that the samples do not change in their morphology in different solvents. However, deuterated heptane was a surprisingly poor solvent. (NPLs were only sparingly soluble in deuterated octane, which is not shown.) This is especially surprising given that most demonstrations of isotopic solubility effects are in protic solvents (e.g.H_2O *versus* D_2O).[30] Toluene is also a poor solvent for NPLs in both deuterated and natural abundance forms. In both heptane and toluene dispersions, aggregation is evidenced from substantial scattering in the optical spectrum in Figure 2b, analyzed quantitatively in Supporting Information Table S1. This remains an important consideration for

interpreting the results as a poorly-solvated colloid will resembled a solid film.

IPEP dynamics for nine solvents and a solid film are shown in Figure 3a. The dynamics traces are probed at the heavy-hole induced absorption feature, which is the strongest and most spectrally isolated Δα signal. Initially in all samples, time zero is marked by a strong, optical Stark effect induced by the infrared pump passing through the sample. In carbon disulfide and chlorinated solvents, there is a much longer broadband transient signal lasting up to 3 ps which we speculate may arise from non-linear optical responses in those solvents, consistent with the wide use of carbon disulfide in Kerr gating. For all measurements, the incident IR fluence was kept at 3.7 mJ·cm⁻². The absorbed fluence is challenging to calculate for all of the samples, due to large solvent absorption for solvents with lower deuteration purities (See Figure 2a), but previous measurements demonstrated that the dynamics of IPEP measurements are not strongly affected by the pump fluence in the regime used here.[21]

To capture both the rise and decay of the transient absorption signal, normalized Δα traces were fitted to a function convoluting an exponential rise (τ_{rise}) and exponential decay (τ_{decay}) of the form

$$\Delta\alpha(t) = A\left(1 - e^{-t/\tau_{rise}}\right)\left(e^{-t/\tau_{decay}} + B\right).$$

Fits to the dynamics data in Figure 3a are shown with solid lines with the resulting extracted information plotted in Figures 3b to 3d. The rise times of the samples estimated from the fitting procedure were similar for each of the solvents, with the times varying between 10 and 12 ps, as shown in Figure 3b. The rise time of the solid film, however, was slower at 17±1.5 ps. (We note that this time is longer

than in our previously reported measurements,[21] which may reflect the influence of surface graft density on this different sample.[19]) On this basis, it appears that solvation of the ligand layer coating of a nanocrystal facilitates heat transfer from the ligand to the inorganic core. Another possible interpretation is that loss of heat to the surroundings in the solvated samples cuts down the time available (or driving force) for heat transfer to the inorganic core from the ligands. The absence of composition-specific trends in the examined solvents suggests that the vibrational structure of the solvent is not determinate for heat transfer, but rather the enhanced configurational freedom of solvated ligands facilitates transfer, particularly compared to the compacted solid state.[31,32] Previous works on polymer systems have demonstrated the influence of alignment as a means to higher thermal conductivities.[29] However, heat transport within the individual ligands is reportedly ballistic, based upon study of self-assembled monolayers.[33] It is far less clear that the tightly-packed configuration of surface ligands is advantageous for *interfacial* heat transport; these experimental results suggest that it is not beneficial.

After the equilibration of heat from the hot ligands to the cold inorganic nanocrystals, the hot nanocrystal-ligand complex undergoes a slower equilibration with the surrounding environment. Many factors may affect the rate of heat outflow from the nanocrystal-ligand complex including the vibrational structure of the solvent and the penetration of the solvent into the ligand layer. Decay times for the solution samples shown in Figure 3c vary from 150 ps to 320 ps. (A small, fast decay is observed in the solid film, followed by a long-lived plateau which persists beyond our measurement window.) Previous measurements of heat outflow from electronically excited metal nanoparticles to solvents is also hundreds of picoseconds.[10–12,14] The differences observed here are not attributable to different diffusivities of the solvents: characteristic diffusion lengths are similar among the different solvents (Supporting Information Figure S3) and show no systematic relationship to the cooling times. Instead, the atomic composition and structure are more likely the underlying reasons for the observed variation.

Similar to most inorganic materials, the phonons of the CdSe NPLs are primarily low-energy (< 30 meV), which accounts for its infrared transparency. In contrast, many vibrations of the organic ligands occur between 0.1 and 0.4 eV. Due to their heavy atoms, halogenated solvents and carbon disulfide are expected to have a vibrational density of states which is closer to that of CdSe than hydrocarbon solvents. In IPEP experiments, halogenated solvents show nearly identical, longer decay times near 315 ps, and carbon disulfide shows a cooling time of 284±14 ps. The relatively slow outcoupling of heat in these solvents experimentally demonstrates that the organic ligand layer serves as an important intermediary as predicted in previous simulations[19,34] and that direct transfer of heat from inorganic core to the solvent does not play a significant role for this sample.

Following this logic, heat outcoupling to hydrocarbon solvents, which have a vibrational and conformational structure similar to oleate ligands, should be faster. It is indeed found that cooling τ_{decay} times for deuterated hexane, cyclohexane, and methylcyclohexane fall between 150 and 200 ps. However, deuterated toluene and heptane showed heat decay time-scales of 265 ps and 282 ps,

respectively, which undermines the clarity of structure-property relationships in the cooling process. Referring back to Figure 2b, these are also the hydrocarbon solvents which showed relatively poorer solubility.

Although poor solvents may have vibrational structure matching the ligands, they are less likely to adopt the complementary conformation for heat flow between ligand and solvent which is critical in molecular dynamics simulations.[19,34] In the most extreme case, a poorly solvated colloid resembles a solid film. Contributions from aggregated nanocrystals increase the apparent lifetime of the cooling process. More subtly, a poor solvent penetrates the ligand layer less, leading to slowed heat transfer. Thus, in NPLs with the best solvents which have a vibrational and molecular structure most commensurate with the ligands, heat transfer appears most rapid.

In addition to extracting the dynamics parameters, an estimate of the maximum change in temperature (ΔT_{max} shown in Figure 3e) for each of the samples was calculated from the peak $\Delta\alpha$ spectrum, using a calibration curve obtained in static heating measurements (see Figure 1c and Supporting Information Figure S5). Due to differences in the resolution of the static spectra and transient IPEP spectra, an integral of the heavy hole induced absorption feature was used for the calibration of temperature. The temperature rise of the sample observed in all solutions was considerably smaller than the temperature rise observed in a solid film. This partially reflects attenuation of the pump pulse lost to solvent absorption—which is most prominent in imperfectly deuterated hydrocarbon solvents—but even for highly infrared transparent solvents like carbon tetrachloride, the temperature rise is still much smaller. The cooling pathway not strongly evident in solids but present in solutions, we suggest, suppresses the maximal temperature rise of the nanocrystals. These results also convey that the cooling times reported in Figure 1c reflect a small temperature differentials. Somewhat surprisingly, considering Newton's law ($dT/dt = -k\Delta T$) that cooling rates are proportional to the temperature difference of two bodies, our results do not show an unambiguous dependence based upon the magnitude of the temperature change. More examination is necessary to make an affirmative conclusion, but it is hypothesized that this is because all of the temperature differentials in this work are small (and similar in an absolute sense) and that differences in the proportionality term of Newton's law override changes in ΔT under these experimental conditions.

Conclusions

IPEP experiments reveal that, to first order, heat flow processes in all solvents look similar: solvated NPLs cool in hundreds of picoseconds whereas a solid film shows very little cooling of the nanocrystal-ligand complex over 2 ns. These results emphasize that a typical nanocrystal solid is a particularly poor environment for heat outflow. A comparison of the different solvents shows rather little impact on the transfer of heat from ligands to inorganic cores. However, outflow of heat from the nanocrystal-ligand complex to the solvent matrix is impacted, by a factor of approximately two in the best hydrocarbon solvents *versus* halogenated solvents and carbon disulfide. This work provides experimental confirmation that matching both

the vibrational and molecular structure of the ligand layer facilitates heat transfer from solvated colloidal nanocrystals into solution. Additional impacts of ligand coverage remain to be further investigated.

Conflicts of interest

There are no conflicts to declare.

Acknowledgements

Notes and references

1   S. Coe-Sullivan, W. Liu, P. Allen and J. S. Steckel, *ECS J. Solid State Sci. Technol.*, 2012, **2**, R3026–R3030.

2   Y. Zhao, C. Riemersma, F. Pietra, R. Koole, C. de M. Donegá and A. Meijerink, *ACS Nano*, 2012, **6**, 9058–9067.

3   H. Moon, C. Lee, W. Lee, J. Kim and H. Chae, *Adv. Mater.*, 2019, 1804294.

4   V. L. Colvin, M. C. Schlamp and A. P. Alivisatos, *Nature*, 1994, **370**, 354–357.

5   C. Dang, J. Lee, C. Breen, J. S. Steckel, S. Coe-Sullivan and A. Nurmikko, *Nat. Nanotech.*, 2012, **7**, 335–339.

6   X. H. Huang, I. H. El-Sayed, W. Qian and M. A. El-Sayed, *J. Am. Chem. Soc.*, 2006, **128**, 2115–2120.

7   W. Kim, J. Zide, A. Gossard, D. Klenov, S. Stemmer, A. Shakouri and A. Majumdar, *Phys. Rev. Lett.*, 2006, **96**, 1–4.

8   W. Ong, S. M. Rupich, D. V Talapin, A. J. H. Mcgaughey and J. A. Malen, *Nat. Mater.*, 2013, **12**, 410–415.

9   J. P. Feser, E. M. Chan, A. Majumdar, R. A. Segalman and J. J. Urban, *Nano Lett.*, 2013, **13**, 2122–2127.

10   Z. Ge, D. G. Cahill and P. V. Braun, *J. Phys. Chem. B*, 2004, **108**, 18870–18875.

11   S. C. Nguyen, Q. Zhang, K. Manthiram, X. Ye, J. P. Lomont, C. B. Harris, H. Weller and A. P. Alivisatos, *ACS Nano*, 2016, **10**, 2144–2151.

12   G. V Hartland, *Chem. Rev.*, 2011, **111**, 3858–3887.

13   B. T. Diroll, P. Guo, R. P. H. Chang and R. D. Schaller, *ACS Nano*, 2016, **10**, 10099–10105.

14   A. J. Schmidt, J. D. Alper, M. Chiesa, G. Chen, S. K. Das and K. Hamad-Schifferli, *J. Phys. Chem. C*, 2008, **112**, 13320–13323.

15   J. H. Hodak, A. Henglein and G. V. Hartland, *J. Chem. Phys.*, 1999, **111**, 8613–8621.

16   S. Link and M. A. El-Sayed, *J. Phys. Chem. B*, 1999, **103**, 8410–8426.

17   M. S. Kirschner, D. C. Hannah, B. T. Diroll, X. Zhang, M. J. Wagner, D. Hayes, A. Y. Chang, C. E. Rowland, C. M. Lethiec, G. C. Schatz, L. X. Chen and R. D. Schaller, *Nano Lett.*, 2017, **17**, 5314–5320.

18   D. C. Hannah, N. J. Dunn, S. Ithurria, D. V. Talapin, L. X. Chen, M. Pelton, G. C. Schatz and R. D. Schaller, *Phys. Rev. Lett.*, 2011, **107**, 13–16.

19   D. C. Hannah, J. D. Gezelter, R. D. Schaller and G. C. Schatz, *ACS Nano*, 2015, **9**, 6278–6287.

20   S. Ithurria, M. D. Tessier, B. Mahler, R. P. S. M. Lobo, B. Dubertret and A. L. Efros, *Nat. Mater.*, 2011, **10**, 936–941.

21   B. T. Diroll, P. Guo and R. D. Schaller, *Nano Lett.*, 2018, **18**, 7863–7869.

22   P. Kukura, D. W. McCamant and R. A. Mathies, *Annu. Rev. Phys. Chem.*, 2007, **58**, 461–488.

23   P. Reddy, K. Castelino and A. Majumdar, *Appl. Phys. Lett.*, 2005, **87**, 1–3.

24   E. T. Swartz and R. O. Pohl, *Rev. Mod. Phys.*, 1989, **61**, 605–668.

25   M. D. Losego and D. G. Cahill, *Nat. Mater.*, 2013, **12**, 382–384.

26   W.-L. L. Ong, S. Majumdar, J. A. Malen and A. J. H. McGaughey, *J. Phys. Chem. C*, 2014, **118**, 7288–7295.

27   R. Y. Wang, R. A. Segalman and A. Majumdar, *Appl. Phys. Lett.*, 2006, **89**, 17–20.

28   K. M. Stocker and J. D. Gezelter, *J. Phys. Chem. C*, 2013, **117**, 7605–7612.

29   S. Shen, A. Henry, J. Tong, R. Zheng and G. Chen, *Nat. Nanotechnol.*, 2010, **5**, 251–255.

30   W. A. van Hook and L. P. N. Rebelo, in *Development and Applications in Solubility*, ed. T. M. Letcher, RSC Publishing, Cambridge, 2007, pp. 78–93.

31   N. Geva, J. J. Shepherd, L. Nienhaus, M. G. Bawendi and T. Van Voorhis, *J. Phys. Chem. C*, 2018, **122**, 26267–26274.

32   B. T. B. T. Diroll, K. M. K. M. Weigandt, D. Jishkariani, M. Cargnello, R. J. R. J. Murphy, L. A. L. A. Hough, C. B. C. B. Murray and B. Donnio, *Nano Lett.*, 2015, **15**, 8008–8012.

33   Z. Wang, J. a. Carter, A. Lagutchev, K. K. Yee, N. H. Seong, D. G. Cahilll and D. D. Dlott, *Science*, 2007, **317**, 787–790.

34   S. Kuang and J. D. Gezelter, *J. Phys. Chem. C*, 2011, **115**, 22475–22483.

ARTICLE

Table of Contents Graphic and Description:
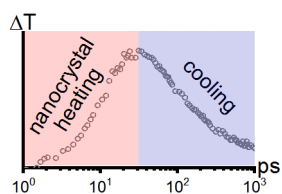
Infrared pump, electronic probe (IPEP) spectroscopy is used to study matrix-dependent heat transfer processes of colloidal semiconductor nanocrystals.